JOURNAL OF PROPULSION AND POWER
Vol. 23, No. 4, July–August 2007

Aerodynamic Inverse Design for Viscous Flow in Turbomachinery Blading

Kasra Daneshkhah* and Wahid Ghaly†
Concordia University, Montreal, Quebec H3G 1M8, Canada

DOI: 10.2514/1.27740

An inverse design method for turbomachinery blading based on a time-accurate solution of the compressible viscous flow equations on a time-varying geometry is presented. The blade pressure loading and thickness distributions are the prescribed design parameters. The blade profile is modified as it moves at a virtual velocity distribution that would make the momentum flux on the blade surfaces equal to the flux corresponding to the prescribed loading distribution. The unsteady flow due to the blade motion is simulated by solving the Reynolds-averaged Navier–Stokes equations that are discretized using a cell-vertex finite volume method in which an arbitrary Lagrangian-Eulerian formulation is used to account for the mesh movement and deformation during the design procedure. The method is first verified by inversely designing an existing blade using its loading distribution as the design target and starting from a profile that has a different camberline. The robustness, flexibility, and usefulness of this design method are demonstrated by redesigning a subsonic turbine and a transonic compressor blade for which, for the latter case, the conventional quasi-steady approach failed. The redesign cases demonstrate that the blade aerodynamic performance can be improved by carefully tailoring the target loading distribution.

Nomenclature

a	=	speed of sound
c	=	axial chord length
$\boldsymbol{F}$	=	convective flux vectors
$f(x)$	=	blade camberline profile
$\boldsymbol{G}$	=	viscous flux vectors
M	=	Mach number
$\dot{m}_r$	=	reduced mass flow rate
$\boldsymbol{n}$	=	surface normal vector
p	=	pressure
Re	=	Reynolds number
s/c	=	cascade solidity
$T(x)$	=	blade thickness distribution
t	=	time
u, v	=	Cartesian velocity components
α	=	flow angle
γ	=	stagger angle
ρ	=	density
Ω	=	control volume

Subscripts

d	=	design
n	=	normal
o	=	total
v	=	virtual
1,2	=	inlet, exit

Superscripts

$+$	=	blade pressure surface
$-$	=	blade suction surface

Received 18 September 2006; revision received 9 March 2007; accepted for publication 9 March 2007.

*Research Associate, Mechanical and Industrial Engineering Department, EV 14-115, 1455 de Maisonneuve West. Member AIAA.

†Associate Professor, Mechanical and Industrial Engineering Department, EV 4-151, 1455 de Maisonneuve West. Senior Member AIAA.

I. Introduction

AERODYNAMIC analysis of the flow in the blade row passages of modern gas turbine engines is routinely performed using computational fluid dynamics (CFD). However, aerodynamic design methods using mainstream CFD schemes have not progressed as fast as analysis methods and have not been used as a common design tool in engineering practice. Some designers still use the direct (or analysis) approach, in which the blade performance is evaluated and the blade geometry is then modified based on empirical rules to reach a target performance. This approach can be very time-consuming and sometimes ineffective.

In situations in which the required blade performance is known in some detail (e.g., the pressure loading or the pressure distribution on the blade surfaces), inverse methods are probably the best and most efficient approach to use. In the inverse shape design problem, the flow-governing equations are recast such that the required detailed performance is prescribed, and the corresponding blade shape and flowfield are obtained simultaneously as part of the inverse design solution. The implementation of these methods requires modifications of the CFD flow solver and/or boundary conditions. The computational time taken by inverse methods is comparable with that taken by analysis methods, which makes inverse methods attractive as design tools for shaping turbomachinery blades for a given performance.

Two-dimensional inverse blade design methods typically assume a target pressure [1–6], Mach number [7], or velocity distribution [8] along the blade surfaces. Other inverse methods assume a target distribution of the blade pressure loading and thickness distribution [9–11]. Starting from an initial guess for the blade shape, these methods use a flow simulation tool to compute the flowfield, then the difference between the calculated and the target distributions (e.g., pressure distributions on the blade surfaces) is used to change the blade shape, and the process is repeated until convergence.

Most inverse design methods solve the problem as a quasi-steady flow problem and do not account for the blade movement in the formulation. The errors resulting from the quasi-steady assumption will propagate into the new blade shape, which will affect the pressure field computed at the next iteration. In some design approaches and for some target pressure distributions, such errors can result in an inaccurate blade shape or in the divergence of the iterative process. The elimination of these errors by using a time-accurate formulation will result in a more robust method that can handle relatively difficult design cases. This fact is verified in part by Demeulenaere et al. [6] who used a time-marching (but not time-

accurate) approach in which they accounted for the mesh movement into the formulation, thus improving the convergence of the inverse method.

The inverse blade design methods for viscous flows were shown to be quite efficient [5,6,11,12], however, they still carry some traces of inviscid flow implementation. Some methods [5] involve viscous–inviscid interaction (so that the metal profile has to be obtained by subtracting the displacement thickness), some [11,12] use the tangency condition to find the new blade camberline, whereas other methods [6] use the transpiration approach in which a velocity tangent to the blade is needed. In all of the preceding methods, it is assumed that the flow is attached and the boundary layers are well-behaved, so that the velocity at the edge of the boundary layer can be used to get the new blade profile.

Recently, Daneshkhah and Ghaly [13], developed an inverse design method for viscous flow in which the blade modification is based on a virtual wall movement computed from the difference between the current and target pressure distributions on the blade surfaces through a momentum flux balance. This approach is independent of the flow tangency condition and can be applied directly to viscous flow. The virtual-wall-movement method was originally proposed by Thompkins and Tong [1] and was implemented into an Euler solver assuming quasi-steady flow. It was applied to design transonic compressor cascade in inviscid flow [2]. Application of this method to viscous flow reported by Yang and Ntone [3] showed large discrepancies between the prescribed and computed pressure distributions, and the blade shape obtained for subsonic flow was rather wavy. Moreover, that implementation [3] was not successful in designing transonic blades. The authors [13] recently implemented the virtual-wall-velocity approach in a consistent manner into the Reynolds-averaged Navier–Stokes (RANS) equations using a Lagrangian-Eulerian (ALE) formulation that accounts for the mesh movement and deformation. During the design computation, the blade moves with that virtual velocity toward a steady shape that would satisfy the prescribed loading distribution. The unsteady flow due to the blade motion is simulated using a time-accurate finite volume (FV) method of the Jameson type [14]. The method was successfully verified for viscous flow and was applied to the redesign of subsonic and transonic turbomachinery cascades [13].

In this paper, the scheme devised by the authors [13] is modified so that the blade loading and thickness distributions are the prescribed design parameters. This formulation allows for a better control of the blade aerodynamic performance and provides more control over the blade structural and manufacturing constraints. The new choice of design parameters is first verified by designing an existing transonic compressor cascade using its loading distribution as the design target and starting from a geometry that has the same thickness distribution but a different camberline. The inverse method is then applied to the redesign of a transonic compressor and a subsonic turbine blade to obtain a prescribed loading and thickness distributions. The effect of using a time-accurate iterative solution scheme on robustness, accuracy, and consistency is emphasized, and the approach used to prescribe the blade loading that would improve or eliminate undesirable flow features is discussed in some detail.

II. Governing Equations and Solution Method

The RANS equations are used to describe the flowfield both in the analysis and design modes of the computations. The governing equations are written for unsteady flow in a domain with moving and deforming boundaries using an arbitrary ALE formulation. For 2-D flow, these equations can be written in integral form on discrete control volumes as

$$\frac{\partial}{\partial t}\iint_{\Omega(t)} \boldsymbol{w}\,d\Omega + \oint_{\partial\Omega(t)} \boldsymbol{F}\cdot\boldsymbol{n}\,d\Gamma = \frac{1}{Re}\oint_{\partial\Omega(t)} \boldsymbol{G}\cdot\boldsymbol{n}\,d\Gamma \qquad (1)$$

where $\boldsymbol{n}$ represents the outward unit vector of the control volume boundary $\partial\Omega(t)$, and $\boldsymbol{w}$ is the vector of conservative variables.

The spatial discretization of the governing equations is performed using a cell-vertex finite volume method of Jameson's type on a fully unstructured triangular mesh [15]. The method uses an explicit Runge–Kutta time-stepping procedure to obtain the steady-state solution in which local time-stepping and implicit residual smoothing are employed for convergence acceleration. During the design process, a time-accurate solution is ensured using a dual-time-stepping scheme [14]. The grid velocities for a moving mesh are computed from the space conservation law (SCL) [16]. The inflow and outflow boundary conditions are based on a linearized one-dimensional characteristic method [17]. The Baldwin–Lomax model [18], adapted for the use on unstructured meshes [19], is used for turbulence closure.

III. Inverse Design Method

The current approach to inverse design is to replace the fixed-wall boundary condition with a moving-wall boundary condition; this movement is controlled by a virtual velocity distribution [1]. The transient momentum flux on the blade surfaces, assuming a virtual velocity distribution, has the following form:

$$\boldsymbol{F} = \begin{bmatrix} (\rho u^v u^v + p)n_x + (\rho u^v v^v)n_y \\ (\rho u^v v^v)n_x + (\rho v^v v^v + p)n_y \end{bmatrix} \qquad (2)$$

where $\boldsymbol{v}^v = (u^v, v^v)$ is the virtual velocity vector and $\boldsymbol{n} = (n_x, n_y)$ is the surface normal vector. At design conditions, the virtual velocity distribution vanishes and the only contribution to steady-state momentum fluxes is through the target (design) pressure p^d, that is,

$$\boldsymbol{F}^d = \begin{bmatrix} p^d n_x \\ p^d n_y \end{bmatrix} \qquad (3)$$

The virtual velocity can be calculated by requiring that

$$\boldsymbol{F} = \boldsymbol{F}^d \qquad (4)$$

which can be solved directly to obtain the virtual velocity components:

$$v^v = \pm\left(\frac{n_y^2}{n_x^2 + n_y^2}\frac{|p^d - p|}{\rho}\right)^{\frac{1}{2}} \qquad u^v = v^v\frac{n_x}{n_y} \qquad (5)$$

The signs of u^v and v^v are chosen such that an excess predicted pressure is balanced by a positive wall velocity. For convenience, the component of the virtual velocity normal to the wall was chosen to be the wall velocity and is given by

$$v_n^v = \boldsymbol{v}^v\cdot\boldsymbol{n} \qquad (6)$$

It follows that the wall displacement δs in a time interval δt is equal to

$$\delta s = -\omega\delta t v_n^v \qquad (7)$$

where δt is the physical time step and ω is a relaxation factor. The negative sign in Eq. (7) indicates that the wall moves in a direction opposite to v_n^v.

A stability analysis of the scheme shows that the virtual velocity distribution must be heavily under-relaxed to ensure convergence of the scheme to a steady-state solution [1]. The relaxation factor is found to have the following form:

$$\omega = \varepsilon\cdot(1/a)\sqrt{|\Delta p|/\rho} \qquad (8)$$

where ε is a constant. The suggested value of ε was 0.01–0.02 [2], however, the present implementation allows for higher values of ε: namely, $\varepsilon = 0.2$ or 0.1 for subsonic or transonic outflow design cases.

A. Inverse Design Implementation

To prescribe a loading distribution as the design input, the surface pressure distributions that would satisfy that loading need to be computed, because the numerical implementation requires these

pressures to compute the virtual-wall velocity. The target pressure distributions can be computed from the prescribed loading distribution as

$$p_d^{\pm} = \tfrac{1}{2}[(p^+ + p^-) \pm \Delta p_d] \tag{9}$$

where p^+ and p^- are the calculated values. In some cases, Eq. (9) may result in a nonphysical value for p_d^+: namely, $p_d^+ > 1$ during the convergence process. Given that the pressure distribution on the pressure side is usually less sensitive to changes in geometry, then for such cases, p_d^+ is taken to be that prevailing from the current iteration, so that

$$p_d^+ = p^+ \quad \text{and} \quad p_d^- = p_d^+ - \Delta p_d \tag{10}$$

Note that p^+ will change with the iterations as the tangential thickness is fixed.

To satisfy the imposed blade thickness, the new blade shape is generated as follows. The camberline $f(x)$ is displaced by the average change in blade shape on both blade surfaces obtained from Eq. (7). The imposed blade thickness is then added onto this new camberline, hence generating the blade pressure side (PS) and suction side (SS) profiles.

$$f(x)_{\text{new}} = f(x)_{\text{old}} \pm 0.5(\delta s^+ + \delta s^-) \tag{11}$$

$$y(x)_{\text{new}}^{\pm} = f(x)_{\text{new}} \pm 0.5T(x) \tag{12}$$

To ensure a smooth blade profile, the blade camberline $f(x)_{\text{new}}$ was smoothed before generating the blade profiles $y(x)_{\text{new}}^{\pm}$ in the following way:

$$f_j = f_j + \omega_s[|f_{j+1} - f_j|(f_{j+1} - f_j) + |f_{j-1} - f_j|(f_{j-1} - f_j)] \tag{13}$$

where j refers to discrete points on the blade camberline. A typical value for the smoothing coefficient is $\omega_s = 0.2$. This smoothing eliminates small geometry oscillations that can slow down the global convergence. However, the correct blade camberline for an arbitrary prescribed loading may not be genuinely smooth and the application of Eq. (13) may introduce a real position error. Therefore, a careful balance must be maintained between smoothing out the profile and producing the specified pressure distribution.

B. Inverse Design Algorithm

The preceding design technique is implemented into the unsteady RANS equations in which the blade movement is the source of unsteadiness. After each geometry-modification step, a time-accurate solution is obtained for the flowfield. This iteration procedure is substantially different from that of the conventional quasi-state approach. The time-accurate solution eliminates the errors associated with the flow unsteadiness, hence it significantly improves the scheme robustness. Figure 1 shows the inverse design iterative process. Starting from a semiconverged solution on a trial geometry and a target loading distribution, a virtual velocity distribution is computed from Eqs. (5) on the blade surfaces from which the local geometry modifications are deduced. After the geometry modifications, the computational mesh is adjusted using transfinite interpolation. The grid displacements and hence the grid velocities are then computed for the entire computational domain using the space conservation law [16]. The unsteady governing equations are marched in pseudotime to converge the local problem and obtain the transient pressure distribution on the modified geometry. The overall computational time for an inverse calculation depends on the number of geometry modifications and the computing time required to obtain the time-accurate solution after each geometry modification. The process is repeated until the L_2 norm of the grid velocities is decreased to the desired tolerance, which ensures that a steady-state condition is reached and the target pressure distribution is achieved on the latest blade profile.

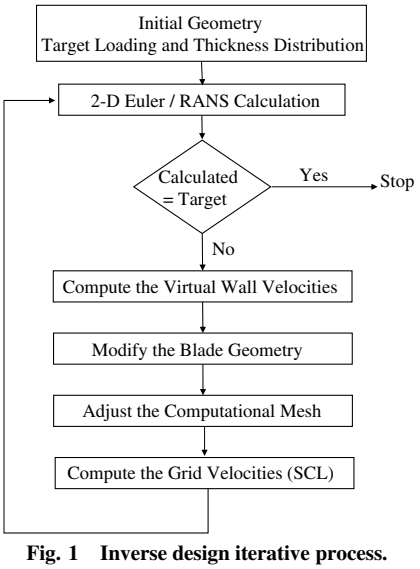

Fig. 1 Inverse design iterative process.

IV. Results

Before using the developed inverse method to redesign blades, it is first assessed for its robustness and uniqueness by inverse designing an existing blade geometry using its loading distribution, obtained from the flow analysis, as the design target. The initial geometry has the same thickness distribution as the target but a different camberline. After the method is verified, its usefulness and flexibility is demonstrated by redesigning a transonic compressor cascade with a relatively large separation region and a subsonic turbine cascade in which a smoother loading distribution is prescribed. A comparison of the time-accurate and quasi-steady iterative formulation is also presented for each case.

A. Method Verification for ONERA Transonic Compressor

In this section, the viscous inverse design method is verified by inversely designing an existing blade (referred to as the target) for which the blade loading and thickness distributions are prescribed. A highly loaded transonic compressor cascade that was experimentally investigated at ONERA [20] was chosen for this verification. The inverse design calculation is initiated with a blade shape that has the same thickness distribution but a different camberline from the target, as depicted in Fig. 2.

The main geometrical characteristics of the cascade and the flow data are listed in Table 1. The initial and target blades are first analyzed by solving the RANS equation. Figure 3 shows the Mach contours for the target blade, for which there is a detached bow shock that impinges on the blade suction side at about 20% chord. The flow remains attached on the blade pressure surface, but it separated at about 75% chord on the blade suction side (see Fig. 4). The blade loading distribution obtained from flow analysis is then used as the design target for the initial blade.

To obtain a unique blade shape for a given target loading, the reduced mass flow rate must also be specified. This can be accomplished implicitly by adjusting the back pressure [21] or explicitly through the choice of inlet boundary conditions; the second approach is used in the present work. Hence, the boundary

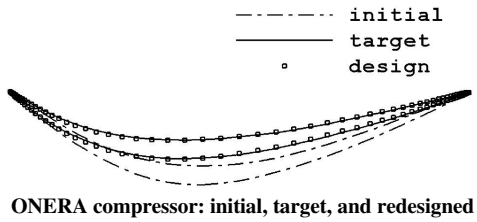

Fig. 2 ONERA compressor: initial, target, and redesigned blades.

Table 1 ONERA compressor cascade data

Inlet flow angle	$\alpha_1 = -38.9$ deg
Exit flow angle	$\alpha_2 \simeq 16$ deg
Blade stagger angle	$\gamma = 0$ deg
Cascade solidity	$s/c = 0.294$
Reynolds number	$Re = 10^6$
Exit isentropic Mach number	$M_{2is} = 0.68$

conditions that are imposed at the inlet and exit boundaries are $\dot{m}_r$, T_{o1}, and α_1 at the inlet and p_2 at the exit.

The resulting blade loading and isentropic Mach number distributions for the initial, target, and inverse calculated cases are presented in Figs. 5 and 6. These figures show clearly that the inverse method has achieved, rather accurately, the target loading and the corresponding pressure distribution on the blade surfaces. The computational time taken by the inverse calculation is almost three times that of an analysis calculation.

To demonstrate the benefits of using a time-accurate simulation on a moving mesh and to describe the evolution of the blade shape from the initial guess to the final steady shape, the design method was carried out using the present time-accurate and the more conventional quasi-steady approaches. Figure 7 shows that the time-accurate simulation converged, whereas the quasi-steady simulation did not converge to a steady shape; rather, it resulted in a breakdown of the flow solver after about 340 geometry-modification steps.

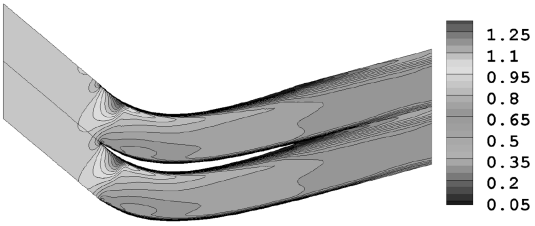

Fig. 3 ONERA compressor: Mach contours.

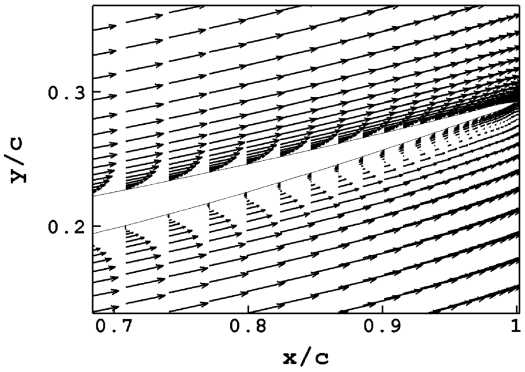

Fig. 4 ONERA compressor: flow separation on the suction side.

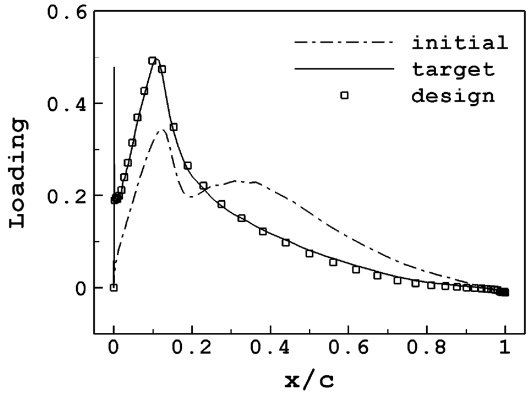

Fig. 5 ONERA compressor: loading distributions.

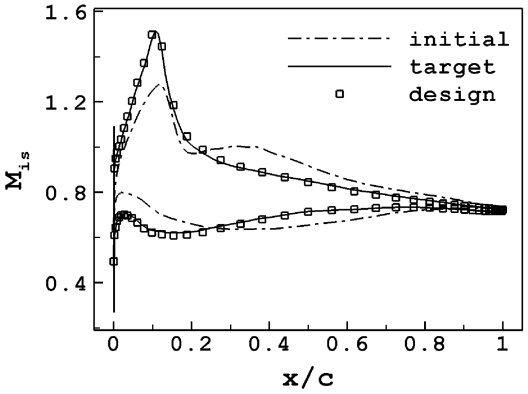

Fig. 6 ONERA compressor: isentropic Mach number distributions.

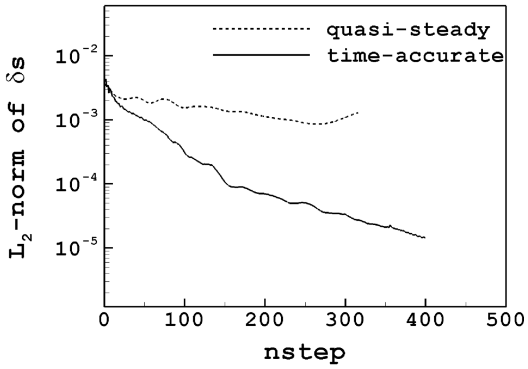

Fig. 7 ONERA compressor: design convergence history.

B. Redesign of NACA Transonic Compressor

The first redesign case is a NACA transonic compressor cascade [22]. Although a number of more recent compressor blades are available in the literature, this case was chosen to demonstrate the significant improvement that can be achieved by the inverse design when the original design is not very efficient and to show the method ability to handle transonic viscous flow cases as well as large separation regions. The cascade geometric characteristics and the flow data are given in Table 2, and the blade geometry is shown in Fig. 8.

This cascade was first analyzed using the RANS equations and the resulting flowfield shows the presence of a shock at about 45% chord, which results in boundary-layer separation over the rest of the blade, as shown in Fig. 9. The original loading distribution was modified such that the target loading has characteristics similar to the original loading, especially near the leading edge and the trailing edge, whereas the shock strength is weakened and the loading is more uniformly distributed over the whole blade. Moreover, the loading distribution results in the same total loading, that is, the same specific work for a rotor or same global flow turning for a stator (provided that the reduced mass flow rate is fixed). The target pressure distributions are then computed during the design process from Eqs. (10).

Table 2 NACA compressor cascade data

Inlet flow angle	$\alpha_1 = 60$ deg
Exit flow angle	$\alpha_2 \simeq 49.6$ deg
Blade stagger angle	$\gamma = 48.3$ deg
Cascade solidity	$s/c = 1.02$
Reynolds number	$Re = 10^6$
Exit isentropic Mach number	$M_{2is} = 0.72$

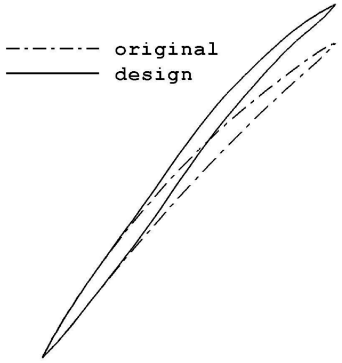

Fig. 8 NACA compressor: original and redesigned blades.

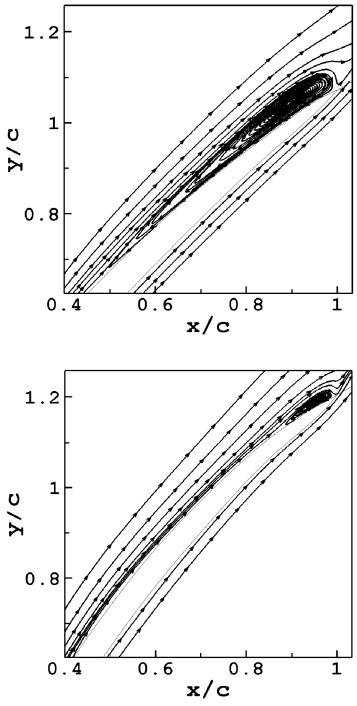

Fig. 9 NACA compressor: streamlines around the original (top) and redesigned (bottom) blades.

Figures 10 and 11 show that the target loading is achieved very well and the calculated isentropic Mach number distributions very well match the originals. The streamlines on the redesigned geometry, shown in Fig. 9, indicate that the separation region on the redesigned blade was decreased from 50% to less than 15% chord. The results also indicate that the static pressure ratio p_2/p_1 across the cascade has increased by 10% and the total pressure loss Δp_o has

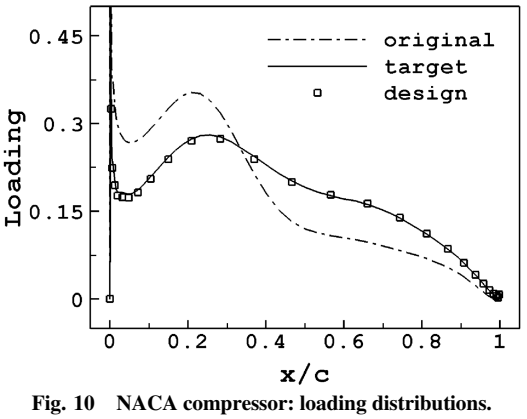

Fig. 10 NACA compressor: loading distributions.

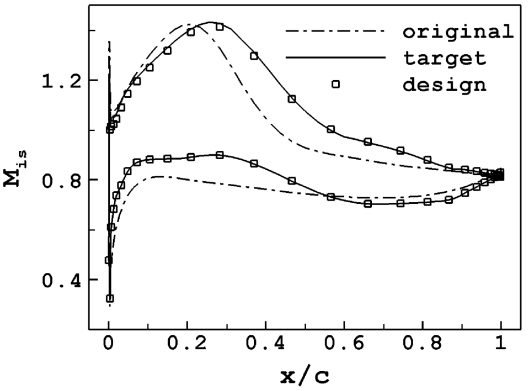

Fig. 11 NACA compressor: isentropic Mach number distributions.

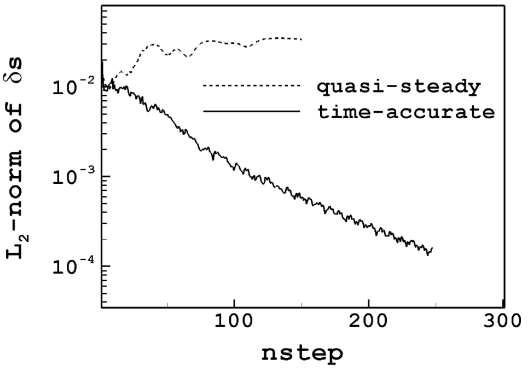

Fig. 12 NACA compressor: design convergence history.

decreased by 24%. Figure 8 shows a comparison of the original and redesigned blade geometries. The blade has almost the same inlet and exit angles, because the original and the redesigned blades have the same total loading and reduced mass flow rate. The redesigned blade has the well-known S-shape configuration so as to weaken the shock strength and hence eliminate or reduce the associated flow separation. Figure 12 shows a comparison between the quasi-steady and the time-accurate convergence histories, in which the former resulted in the breakdown of the flow solver after about 185 geometry-modification steps and produced an unrealistic blade shape. The computational time required for the design calculation is almost three times that of an analysis calculation. This case shows that the design scheme can be effectively used to improve the blade performance in the presence of shock waves and relatively large separation regions by imposing a proper target loading distribution.

C. Redesign of the DFVLR-T106 Subsonic Turbine

The second redesign case is that of a highly cambered blade similar to the DFVLR-T106 subsonic turbine [20]; the cascade characteristics and the flow data are listed in Table 3, and the blade geometry is shown in Fig. 13.

This cascade was first analyzed by solving the RANS equations; the original loading and corresponding pressure distributions are shown in Figs. 14 and 15. The flow is characterized by a region of high diffusion on the suction side between 60 and 70% chord.

Table 3 DFVLR turbine cascade data

Inlet flow angle	$\alpha_1 = 37.7$ deg
Exit flow angle	$\alpha_2 \simeq -63$ deg
Blade stagger angle	$\gamma = 30.8$ deg
Cascade solidity	$s/c = 0.929$
Reynolds number	$Re = 5 \times 10^5$
Exit isentropic Mach number	$M_{2is} = 0.61$

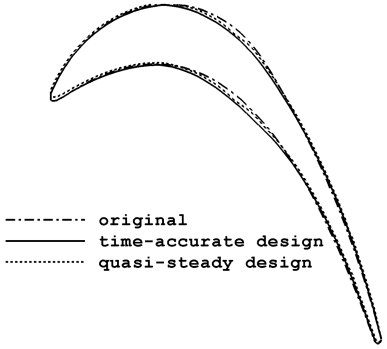

Fig. 13 DFVLR turbine: original and redesigned blades.

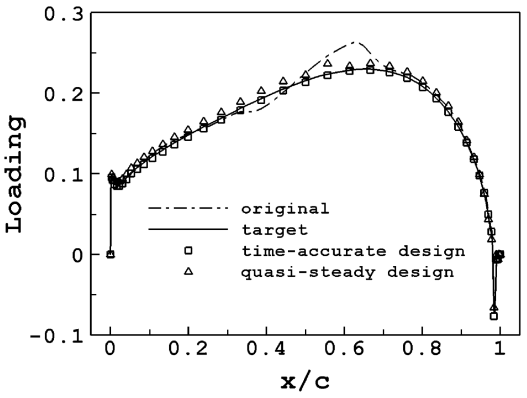

Fig. 14 DFVLR turbine: loading distributions.

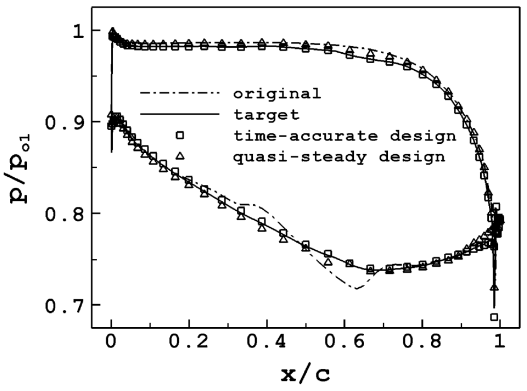

Fig. 15 DFVLR turbine: pressure distributions.

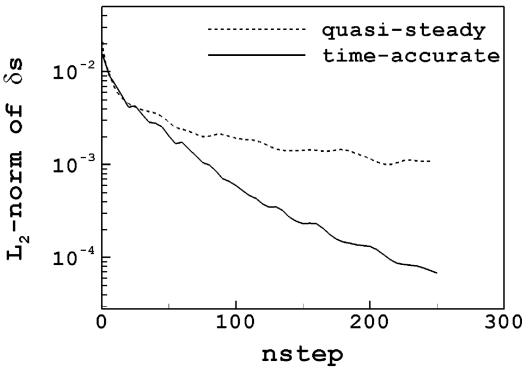

Fig. 16 DFVLR turbine: design convergence history.

The blade was redesigned to give a smoother loading between 30 and 70% chord, whereas the total loading was almost preserved. The convergence history of the time-accurate and quasi-steady methods are compared in Fig. 16. For this case, the quasi-steady design did not result in the breakdown of the flow solver and produced a blade shape after 250 geometry-modification steps. However, the time-accurate approach resulted in a pressure loading that better matches the target (see Figs. 14 and 15), and the resulting blade profile was found to be smoother than that obtained from the quasi-steady approach (see Fig. 13). The original and redesigned blade profiles have almost the same flow turning, which is consistent with imposing the same total loading. For the redesigned blade, the total pressure loss Δp_o and the inflow to outflow pressure ratio p_1/p_2 were reduced by 9.5 and 1.5%, respectively. The inverse design computational time is equivalent to that of two-analysis calculations.

V. Conclusions

An aerodynamic inverse shape design method for turbomachinery blading was presented, assessed, and applied to design linear cascades in 2-D turbulent flow in the subsonic and transonic regimes. The design parameters are the blade loading and their thickness distributions. The method is implemented in a consistent manner into the unsteady RANS equations that are solved on a moving mesh using an ALE formulation. The method robustness and accuracy are first verified by inversely designing an existing transonic compressor cascade. It was shown that the time-accurate scheme was able to redesign a transonic compressor cascade, whereas the conventional quasi-steady approach failed. The usefulness of the inverse method in reshaping the blade to accomplish a given loading distribution was then demonstrated on the redesign of a transonic compressor cascade to reduce the separation bubble by weakening the shock strength and by the redesign of a highly cambered subsonic turbine cascade to achieve a smoother loading distribution. The results indicate that the inverse design method is capable of handling, and can be used to reduce, relatively large separated-flow regions. It was also found that a rather significant improvement in the blade aerodynamic performance can be achieved by carefully tailoring the target loading distribution.

Acknowledgments

The financial support of the National Science and Engineering Research Council (NSERC) of Canada and the Engineering and Computer Science (ENSC) Faculty Support for Research at Concordia University is gratefully acknowledged.

References

[1] Thompkins, W., and Tong, S., "Inverse or Design Calculation for Nonpotential Flows in Turbomachinery Cascades," *Journal of Engineering for Power*, Vol. 104, No. 4, 1982, pp. 281–285.

[2] Tong, S., and Thompkins, W., "A Design Calculation Procedure for Shock-Free or Strong Passage Shock Turbomachinery Cascades," American Society of Mechanical Engineers Paper 82-GT-220, 1982.

[3] Yang, T., and Ntone, F., "Viscous Compressible Flow Direct and Inverse Computation with Illustration," NASA CR-175037, 1986.

[4] Zannetti, L., "A Natural Formulation for the Solution of Two-Dimensional or Axisymmetric Inverse Problems," *International Journal for Numerical Methods in Engineering*, Vol. 22, No. 2, 1986, pp. 451–463.

[5] Giles, M., and Drela, M., "Two Dimensional Transonic Aerodynamic Design method," *AIAA Journal*, Vol. 25, No. 9, 1987, pp. 1199–1205.

[6] Demeulenaere, A., Leonard, O., and Van den Braembussche, R., "A Two-Dimensional Navier–Stokes Inverse Solver for Compressor and Turbine Blade Dasign," *Proceedings of the Institution of Mechanical Engineers, Part A (Journal of Power and Energy)*, Vol. 211, 1997, pp. 299–307.

[7] Leonard, O., and van den Braembussche, R., "Design Method for Subsonic and Transonic Cascades with the Prescribed Mach Number Distribution," *Journal of Turbomachinery*, Vol. 114, No. 3, 1992, pp. 553–560.

[8] Zannetti, L., and Pandolfi, M., "Inverse Design Techniques for Cascades," NASA CR-3836, 1984.

[9] Dang, T., "Inverse Method for Turbomachinery Blade Using Shock-Capturing Techniques," AIAA Paper 95-2465, 1995.

[10] Ahmadi, M., and Ghaly, W., "Aerodynamic Design of Turbomachinery Cascades Using a Finite Volume Method on Unstructured Meshes," *Inverse Problems in Engineering*, Vol. 6, 1998.

[11] Choo, B., and Zangeneh, M., "Development of an (Adaptive) Unstructured 2-D Inverse Design Method for Turbomachinery Blades," American Society of Mechanical Engineers Paper GT-2002-30620, 2002.
[12] Damle, S., Dang, T., Stringham, J., and Razinsky, E., "Practical Use of a 3D Viscous Inverse Method for the Design of Compressor Blade," *Journal of Turbomachinery*, Vol. 121, No. 2, 1999, pp. 321–325.
[13] Daneshkhah, K., and Ghaly, W., "An Inverse Blade Design Method for Subsonic and Transonic Viscous Flow in Compressors and Turbines," *Inverse Problems in Science and Engineering*, Vol. 14, No. 3, 2006, pp. 211–231.
[14] Jameson, A., "Time Dependent Calculations Using Multigrid, with Application to Unsteady Flow Past Airfoils and Wings," AIAA Paper 91-1596, 1991.
[15] Mavriplis, D., Jameson, A., and Martinelli, L., "Multigrid Solution of the Navier Stokes Equations on Triangular Meshes," AIAA Paper 89-0120, 1989.
[16] Demirdzic, I., and Peric, M., "Space Conservation Law in Finite Volume Calculations of Fluid Flow," *International Journal for Numerical Methods in Fluids*, Vol. 8, No. 9, 1988, pp. 1037–1050.
[17] Giles, M., "Nonreflecting Boundary Conditions for Euler Equation Calculations," *AIAA Journal*, Vol. 28, No. 12, 1990, pp. 2050–2058.
[18] Baldwin, B., and Lomax, H., "Thin Layer Approximation and Algebraic Model for Separated Turbulent Flows," AIAA Paper 78-257, 1978.
[19] Mavripilis, D., "Turbulent Flow Calculations Using Unstructured and Adaptive Meshes," *International Journal for Numerical Methods in Fluids*, Vol. 91, No. 13, 1991, pp. 1131–1152.
[20] Fottner, L., "Test Cases for Computation of Internal Flows in Aero Engine Components," AGARD AR-275, 1990.
[21] De Vito, L., den Braembussche, R. V., and Deconinck, M., "A Novel Two-Dimensional Viscous Inverse Design Method for Turbomachinery Blading," *Journal of Turbomachinery*, Vol. 125, No. 2, 2003, pp. 310–316.
[22] Lieblein, S., Lewis, G., and Sandercock, D., "Experimental Investigation of an Axial-Flow Compressor Inlet Stage Operating at Transonic Relative Mach Numbers," NACA RM E52A24, 1952.

F. Liu
Associate Editor